Microstructure and H_2S gas sensing properties of nanocrystalline perovskite-type $La_{0.6}Co_{0.4}Mn_{0.5}Ni_{0.5}O_3$

**A. B. Bodade · Minaz Alvi · A. V. Kadu ·
G. N. Chaudhari**

Abstract Nanocrystalline $La_{1-x}Co_xMn_{1-y}Ni_yO_3$ ($x = 0.2$ and 0.4; $y = 0.1, 0.3$, and 0.5) thick films sensors prepared by sol–gel method were studied for their H_2S gas sensitivity. The structural and morphological properties have been carried out by X-ray diffraction (XRD) and transmission electron microscopy (TEM). Average particle size estimated from XRD and TEM analyses was observed to be 30–35 nm. The gas response characteristics were found to depend on the dopants concentration and operating temperature. The maximum H_2S gas response of pure $LaMnO_3$ was found to be at 300 °C. In order to improve the gas response, material doped with transition metals Co and Ni on A- and B-site, respectively. The $La_{0.6}Co_{0.4}Mn_{0.5}Ni_{0.5}O_3$ shows high response towards H_2S gas at an operating temperature 250 °C. The Pd-doped $La_{0.6}Co_{0.4}Mn_{0.5}Ni_{0.5}O_3$ sensor was found to be highly sensitive to H_2S at an operating temperature 200 °C. The gas response, selectivity, response time and recovery time were studied and discussed.

Introduction

Gas sensors play vital role in detecting, monitoring, and controlling the presence of hazardous and poisonous gases in atmosphere at very low concentrations. An efficient gas sensor must have high gas response and good selectivity at low operating temperature. Gas sensors based on semiconducting oxides are widely used for the application in gas sensing. They offer many advantages such as simple

A. B. Bodade · M. Alvi · A. V. Kadu · G. N. Chaudhari (✉)
Nano Technology Research Laboratory, Department of
Chemistry, Shri Shivaji Science College, Amravati 444602,
Maharashtra, India
e-mail: cgnrao@yahoo.com; gnc4@indiatimes.com

fabrication, low cost, high sensitivity to both reducing and oxidizing gases, etc. Few semiconducting oxide materials being used as gas sensors are ZnO, SnO_2, WO_3, Fe_2O_3, In_2O_3, $NiFe_2O_4$, $MgFe_2O_4$ [1–6], etc. At present, the search for new gas sensing materials and developing the properties of conventional gas sensing materials has become an active research field.

The perovskite-type (ABO_3) $LnMO_3$ oxides having lanthanides (Ln) and tri-valent cations (M) are one of the most applicable materials for catalysis [7, 8], electrodes, and solid electrolytes of fuels cells [9, 10], gas sensors [11, 12], etc. The gas sensing characteristics of the materials can be improved by incorporating few additives into the oxide films [13, 14]. Catalysts like Pt, Pd, Ag, and Ru are often added [14, 15] to the base material to improve the gas response and selectivity.

Hydrogen sulfide (H_2S) is an extremely hazardous, toxic gas. It is a colorless, transparent gas that can be identified in relatively low concentrations, by a characteristic rotten egg odor. At levels of 50–100 ppm, it may cause the human sense of smell to fail. This means that the gas can be present at dangerously at high concentrations, with no perceivable odor. Usually the poisoning caused by H_2S is through inhalation and has toxicity similar to cyanide. Therefore, it is needed to detect and control the H_2S gas for healthy environment. Some well-known materials for H_2S gas sensing are SnO_2–ZnO–CuO [16], SnO_2–Pd [17], SnO_2–Al_2O_3 [18], SnO_2–CuO–SnO_2 [19], $ZnSb_2O_6$ [20], $BaTiO_3$ [21], etc.

In this article, the response of nanocrystalline $La_{1-x}Co_x$ $Mn_{1-y}Ni_yO_3$ ($x = 0.2$ and 0.4, $y = 0.1, 0.3$, and 0.5) was measured to reducing gases at different operating temperatures. The materials were synthesized by sol–gel method. This material was found to an excellent sensor to H_2S gas. Further improvement in response was observed by adding

0.1 wt% Pd to the $La_{0.6}Co_{0.4}Mn_{0.5}Ni_{0.5}O_3$. The gas response characteristics were found to be dependent on the dopants concentration and operating temperature. The structural characteristic of the materials was studied by using X-ray diffraction (XRD) and transmission electron microscopy (TEM).

Experimental details

Materials preparation

Nanocrystalline $La_{1-x}Co_xMn_{1-y}Ni_yO_3$ ($x = 0.2$ and 0.4, $y = 0.1$, 0.3, and 0.5) were prepared by sol–gel method. First, analytical grade $La(NO_3)_3 \cdot 6H_2O$, $Co(NO_3)_2 \cdot 6H_2O$, $Ni(NO_3)_3 \cdot 6H_2O$ and $Mn(NO_3)_3 \cdot 4H_2O$ were weighed accurately and dissolved in deionized water and adding them to an warm aqueous solution (30 °C) of citric acid/ethylene glycol (~ 0.25 mol of citric acid and ~ 1 mol of ethylene glycol) under continuous stirring and to obtain a homogeneous solution. After achieving complete dissolution, the resultant solution was heated with continuous stirring, at 90 °C for 4 h in order to evaporate the excess solvents and promote polymerization. After being heated at 130 °C for 13 h, the solution became highly viscous. The powder was then calcined at 650 °C for 6 h in order to improve the crystallinity of materials.

Appropriate weights of palladium nitrate were dissolved in distilled water and then appropriate weight of above prepared materials was added to this solution. This solution was the stirred on magnetic stirrer. After several hours, the sample was slowly heated to dryness with stirring and then heated at 500 °C for 5 h in air.

Structure and morphological characterization

The synthesized samples were characterized by powder XRD using a Siemens D 5000 diffractometer. The XRD data were recorded by using Cu Kα radiation (1.5406 Å). The intensity data were collected over a 2θ range of 20–80°. The average crystallite size of the samples was estimated with the help of Scherrer equation using the diffraction intensity of all prominent lines [22]. TEM examination of the synthesized powder was performed using an H-800 electron microscope.

Fabrication and analysis of gas sensors

The above-calcined powders were mixed with 2–3% PVA (polyvinyl alcohol) and ethyl alcohol to form paste, then the paste were coated onto an Al_2O_3 tube substrate on which two platinum wires had been installed at each end. The schematic of sensor element used for the gas
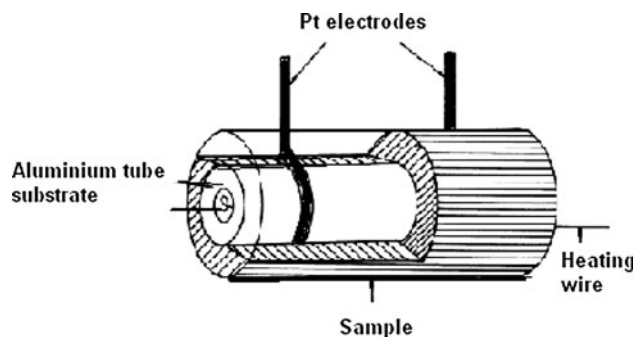

Fig. 1 The schematic of a sensor element used for the gas sensitivity studies

sensitivity studies as shown in Fig. 1. A small Ni–Cr alloy coil was placed through the tube as a heater, which provided operating temperature at 50–350 °C. The temperature was controlled by adjusting the heating power. The alumina tube was about 8 mm in length, 2 mm in external diameter, and 1.6 mm in internal diameter. The sensor is sintered at 400–650 °C for 2–4 h to make it rigid and to impart ceramic properties. Two Pt electrodes have been installed at each end of alumina plates for the measurement of gas sensing properties. The distance between the electrodes was about 1–2 mm. The different test gases are injected into the specimen chamber through an inlet port. The sensor elements, which are equipped with a nichrome heater to provide the necessary temperature and a chromel–alumel thermocouple for temperature monitoring, were fixed inside a specimen chamber made of aluminum for measurement of gas sensing characteristics. Different test gases were injected through an inlet into the specimen chamber. The schematic of gas sensing measurement setup is shown in Fig. 2.

The gas sensing properties of reducing gases such as H_2S, LPG, CO, and NH_3 were measured. The resistance of a sensor was measured in air and in a sample gas. The gas sensitivity (S) is defined as the ratio of the change of resistance in presence of gas (R_g) to that in air (R_a) [23],

$$S = (R_a - R_g)/R_a = \Delta R/R_a \tag{1}$$

where R_a and R_g were the resistance in air and resistance in test gas, respectively. The test temperature range is from 50 to 350 °C, and the gas concentration tested is 300 ppm.

Results and discussion

Structural characterization

Figure 3 (a and b) displays the XRD pattern of the samples $La_{0.6}Co_{0.4}MnO_3$ and $La_{0.6}Co_{0.4}Mn_{0.5}Ni_{0.5}O_3$ calcined at 650 °C, respectively. The XRD pattern shows single phase

Fig. 2 The schematic of gas sensing measurement setup
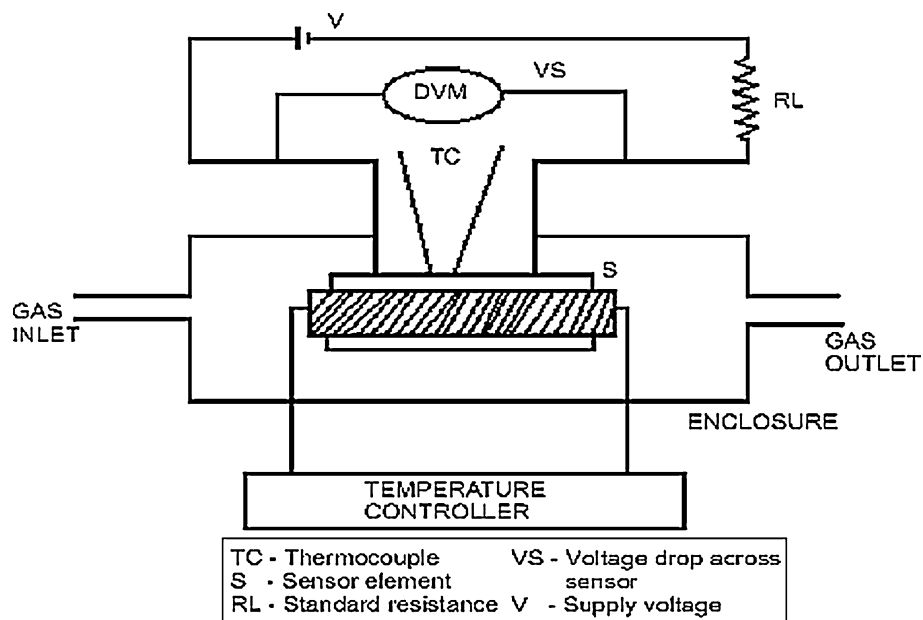
with orthorhombic perovskite-type structure. The sharp diffraction peaks indicate that well-crystallized materials could be achieved by the present synthesis route. The crystallite sizes of powders were calculated by using Scherrer's equation. The obtained D values were about in the range 30–35 nm.

Figure 4 shows TEM micrograph of the sample $La_{0.6}Co_{0.4}Mn_{0.5}Ni_{0.5}O_3$ calcined at 650 °C. The micrographs indicate the uniform distribution of nanosized particles. The average size of particles estimated from the TEM micrograph is 30 ± 2 nm. The measured particle size is consistent with that calculated from the XRD patterns by using Scherrer formula.
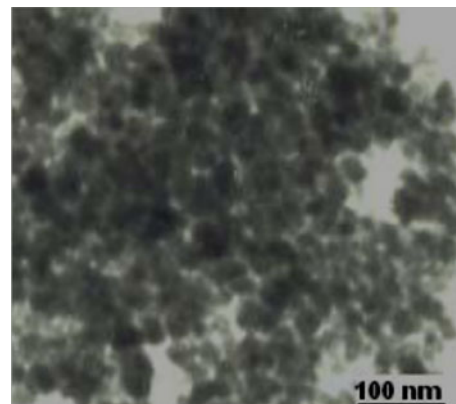
Gas sensing characteristics

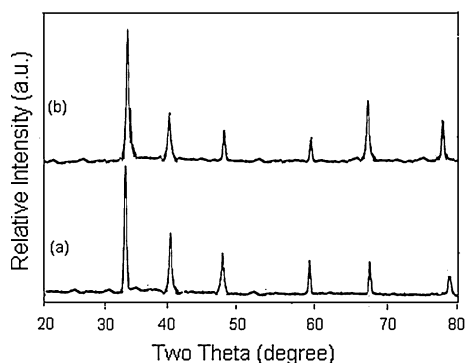In the gas response measurement, the sensor elements were exposed to reducing gases like H_2S, LPG, CO, and NH_3.

Fig. 4 TEM micrograph of $La_{0.6}Co_{0.4}Mn_{0.5}Ni_{0.5}O_3$ calcined at 650 °C

The sensor elements were maintained at different temperatures but gases were introduced in a test chamber at room temperature. The gas response is strongly dependent on operating temperature, type and concentration gas, material composition, and sample microstructure [24]. Figure 5 shows the variation of gas response of undoped (A) $LaMnO_3$ and Co-doped $LaMnO_3$ (B) $La_{0.8}Co_{0.2}MnO_3$ and (C) $La_{0.6}Co_{0.4}MnO_3$ to H_2S gas (300 ppm) with operating temperatures. The undoped $LaMnO_3$ shows lower response (0.45) towards H_2S gas at an operating temperature 300 °C, while the samples $La_{0.8}Co_{0.2}MnO_3$ and $La_{0.6}Co_{0.4}MnO_3$ show higher response (0.52 and 0.60, respectively) towards H_2S gas at an operating temperature 280 °C. Compared with $La_{0.8}Co_{0.2}MnO_3$, $La_{0.6}Co_{0.4}MnO_3$ showed the large response to H_2S gas. The reason may be that the partial replacement of La ions by Co ions at the A-sites is advantageous to adsorption by creating active sites and
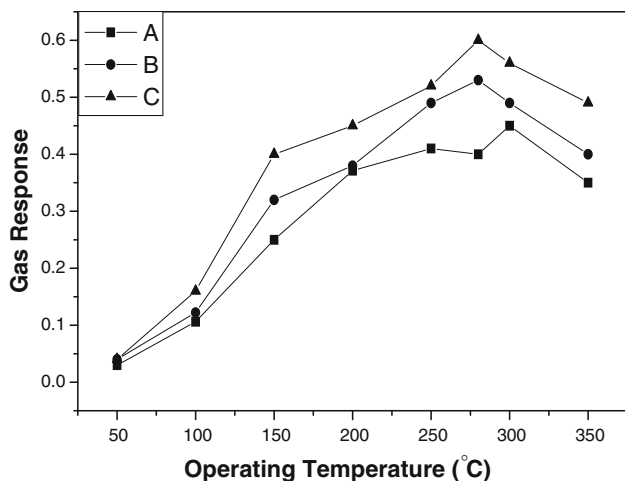

Fig. 3 X-ray diffraction pattern of a $La_{0.6}Co_{0.4}MnO_3$ b $La_{0.6}Co_{0.4}Mn_{0.5}Ni_{0.5}O_3$ calcined at 650 °C

Fig. 5 Gas response versus operating temperature for studied samples calcined at 650 °C for H_2S gas. a $LaMnO_3$, b $La_{0.8}Co_{0.2}MnO_3$ and c $La_{0.6}Co_{0.4}MnO_3$

Fig. 6 Gas response versus operating temperature for studied samples calcined at 650 °C for H_2S gas. a $La_{0.6}Co_{0.4}Mn_{0.9}Ni_{0.1}O_3$, b $La_{0.6}Co_{0.4}Mn_{0.7}Ni_{0.3}O_3$ and c $La_{0.6}Co_{0.4}Mn_{0.5}Ni_{0.5}O_3$

oxidization for H_2S gas. In addition, the partial replacement results in a decrease of grain size and hence in an increase of surface area. Since small grains have relatively large grain boundary areas, the adsorption of gas molecules is relatively high.

It is interesting that the best sensor response towards H_2S gas was obtained for $La_{0.6}Co_{0.4}MnO_3$ sensor with 40% substitution of La by Co, which may due to the highest surface area. The result is not surprising because higher surface area means more surface adsorption sites or surface oxygen anions available to react with the reducing gas [25].

The addition of 3d transition metal oxides is most widely used for improving the gas sensing property [26, 27]. The effect of NiO as a dopant has been reported as a grain growth inhibitor [28, 29]. Figure 6 shows the sensor response as a function of operating temperature for $La_{0.6}Co_{0.4}Mn_{1-y}Ni_yO_3$ ($y = 0.1$, 0.3, and 0.5) studied for various operating temperatures from 50–350 °C. The sensing characteristics indicate that the sensor response to H_2S gas is the highest for Ni ($x = 0.5$) as compared to $x = 0.1$ and 0.3 at an operating temperature 250 °C. The increase in concentration of Ni at the B-site of $La_{0.6}Co_{0.4}MnO_3$ may cause the replacement of Mn by Ni ions of different valence state, leading to the creation of oxygen vacancies to maintain the charge neutrality. The largest response of $La_{0.6}Co_{0.4}Mn_{0.5}Ni_{0.5}O_3$ may be due to more available sites for gaseous oxygen to be adsorbed and in turn to oxidize the test gas. The partial replacement results in a decrease of grain size and hence in an increase of surface area. Owing to the large response and low operating temperature of $La_{0.6}Co_{0.4}Mn_{0.5}Ni_{0.5}O_3$, this material was selected for further studies.

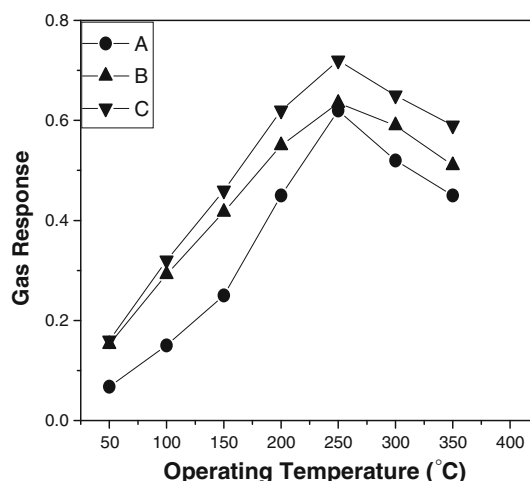The ability of a sensor to respond to a certain gas in the presence of other gases is known as selectivity. At various operating temperatures, the sensor elements were tested against different reducing gases like H_2S, LPG, CO, and NH_3. Figure 7 shows the response of $La_{0.6}Co_{0.4}Mn_{0.5}Ni_{0.5}O_3$ to different reducing gases as a function of operating temperature. The sensor shows the high sensor response towards H_2S gas, and other gases shows low sensor response. It is clear from the graph that the $La_{0.6}Co_{0.4}Mn_{0.5}Ni_{0.5}O_3$ is more selective to H_2S gas than other reducing gases.

The gas response performance can be enhanced by doping small amount of a noble metal catalyst, such as palladium (Pd), which not only promotes gas sensitivity but also reduces the operating temperature [30, 31]. It is well known that noble metal like Pd gets oxidized during the process of doping into the semiconducting oxide. The observed increase in conductivity in Pd-incorporated ferrites is predominantly due to change in work function on
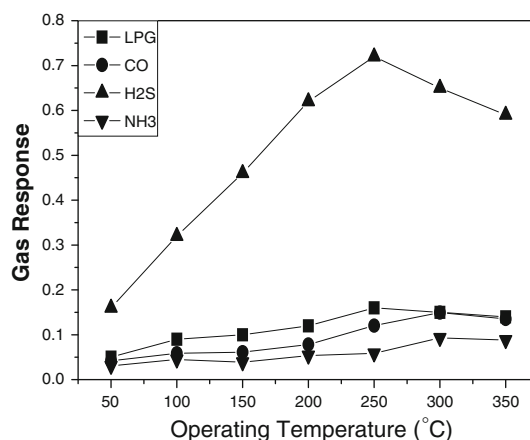

Fig. 7 Cross-sensitivity as a function of operating temperature for $La_{0.6}Co_{0.4}Mn_{0.5}Ni_{0.5}O_3$ calcined at 650 °C for various reducing gases

exposure to reducing gases like H_2S which is termed electronic sensitization [32]. In this case, there is a direct electronic interaction between the metal and the semiconductor surface. The change in work function indicates that each metal in the oxidized form produces a strongly depleted space charge layer on the semiconductor surface, while the interaction with gas promotes the increase in the electron density at the surface when it is reduced to metals. This exhibited as an increase in sensitivity in such noble metal promoted semiconducting oxides surfaces. The effect of Pd doping on the response of H_2S gas at various operating temperatures is shown in Fig. 8. The Pd content was varied from 0.025 to 0.3 wt%. It was observed that the Pd content of 0.1 wt% was the optimum for the maximum response to H_2S gas. The response as the Pd content increased from 0.025 to 0.1 wt% and then decreased above the Pd content of 0.1 wt%.

Figure 9 shows the sensor response of 0.1 wt% Pd-doped $La_{0.6}Co_{0.4}Mn_{0.5}Ni_{0.5}O_3$ calcined at 650 °C as a function of operating temperature. The 0.1 wt% Pd-doped $La_{0.6}Co_{0.4}Mn_{0.5}Ni_{0.5}O_3$ sensors show maximum response towards H_2S at an operating temperature 250 °C. It shows large response to H_2S gas as compared to LPG, CO, and NH_3 at an operating temperature of 200 °C. The figure shows that the sensor not only reduces the operating temperature but also shows high selectivity for H_2S gas.

The enhanced sensor response of the 0.1 wt% Pd-doped $La_{0.6}Co_{0.4}Mn_{0.5}Ni_{0.5}O_3$ can be attributed to the formation of highly reactive species in the reaction [33]. The Pd atoms are weakly bonded with the oxygen gas, and the resulting complex is readily dissociated at relatively low temperature and the oxygen atoms are produced. The created atoms migrate along the surface of the grains. This migration is induced by the catalyst atoms and is known as spillover of the gas ions. Thus, these oxygen atoms capture
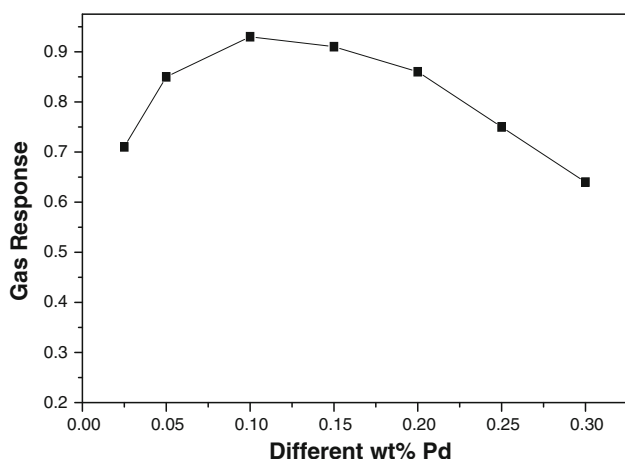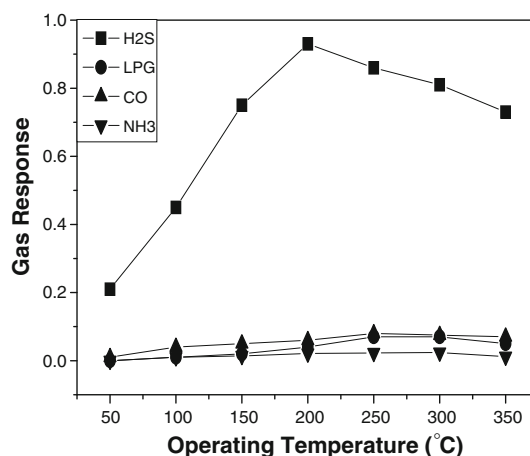
Fig. 9 Gas response as a function of operating temperature for 0.1 wt% Pd-doped $La_{0.6}Co_{0.4}Mn_{0.5}Ni_{0.5}O_3$ calcined at 650 °C for various reducing gases

electrons from the surface layer and acceptor surface states are formed. The reducing gases react with surface oxygen and reduce the resistance. Thus, as there are more numbers of oxygen species there will be more reactions at low temperature. Thus, 0.1 wt% Pd-doped $La_{0.6}Co_{0.4}Mn_{0.5}Ni_{0.5}O_3$ has high response at relatively low operating temperature.

It is known that the sensing mechanism of the oxide materials is surface controlled in which the grain size, surface states, and oxygen adsorption play an important role [34]. The larger surface area generally provides more adsorption–desorption sites and thus the higher gas response. Atmospheric oxygen adsorbs electrons from the conduction band of the sensing metal oxide and occurs on the surface in the form of O^- and O_2^-.

$$O_{2(g)} + e^- \rightarrow O_{2(ads)}^- \tag{2}$$

$$O_{2(ads)}^- + e^- \rightarrow 2O_{(ads)}^- \tag{3}$$
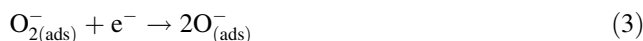
The adsorbed oxygen species play a crucial role in H_2S-sensing. With the introduction of the H_2S gas, it would react with oxygen ions adsorbed on the surface of the sensor. The possible reaction process is as follows:

$$H_2S + 3O_{(ads)}^- \rightarrow SO_{2(g)} + H_2O_{(g)} + 3e^- \tag{4}$$
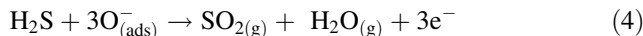
As expected from Eq. 4, the resistance of the nanostructured oxide decreases on contact with H_2S. It is expected that the resistance change upon the exposure to H_2S be mainly due to the resistance change of metal oxide. According to Eqs. 2 and 3, oxygen adsorption reaction occurs prior to H_2S-sensing, creating a thin electron-depleted layer at the surface of metal oxide. As H_2S is adsorbed, electrons are released into the conduction band according to Eq. 4. When reducing gas such as H_2S, comes into contact with the grain boundaries of metal oxides,
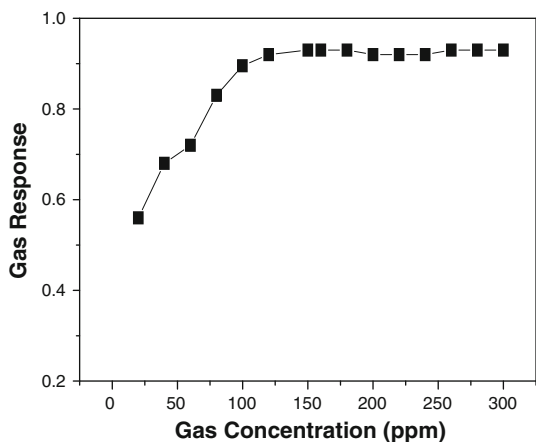
Fig. 8 Gas response versus different wt% Pd-doped $La_{0.6}Co_{0.4}Mn_{0.5}Ni_{0.5}O_3$ calcined at 650 °C for H_2S gas

Fig. 10 Gas response of 0.1 wt% Pd-doped $La_{0.6}Co_{0.4}Mn_{0.5}Ni_{0.5}O_3$ calcined at 650 °C for H_2S gas concentration (in ppm)

Fig. 12 Stability of 0.1 wt% Pd-doped $La_{0.6}Co_{0.4}Mn_{0.5}Ni_{0.5}O_3$-based H_2S gas sensor over time

potential barrier will decrease as a result of oxidation of H_2S and desorption of oxygen. In the present case the decrease in resistivity of metal oxides thick film sensor in the presence of H_2S gas may be explained by the Eq. 4.

Figure 10 shows the response of 0.1 wt% Pd-doped $La_{0.6}Co_{0.4}Mn_{0.5}Ni_{0.5}O_3$ as a function of H_2S gas concentration at 300 ppm. In general, the gas response of the sensor increases with the increase of the concentration of sensing gas in air. For the gas sensor investigated, the magnitude of gas response increased linearly with the H_2S gas concentration from 25 to 100 ppm. It is observed that the sensor has a tendency for the sensitivity to saturate at the gas concentration above 100 ppm. The highest sensitivity was observed at the H_2S gas concentration of 100 ppm. The response and recovery time of the most
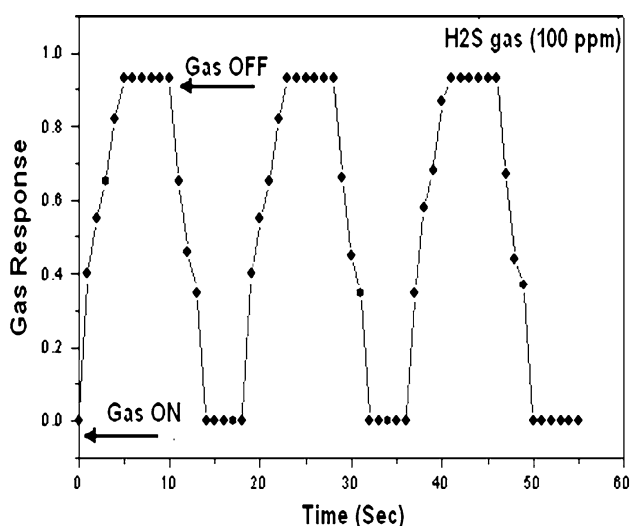
sensitive 0.1 wt% Pd-doped $La_{0.6}Co_{0.4}Mn_{0.5}Ni_{0.5}O_3$ is represented in Fig. 11. The response was quick (5 s) and the recovery time was 20 s, at 200 °C to H_2S gas for 100 ppm gas concentration.

Figure 12 shows the gas response of the sensor to H_2S gas was recorded as a function of time. This figure shows the sensitivity rises from 10 days and then remains relatively stable. The initial increase in sensitivity is believed to be caused by activation and redistribution of the impurities. Repeating absorption and desorption processes and redistribution of Pd in the material improves the activation and enhances the absorption and reaction of H_2S gas, causing gradual increase in the sensitivity and further it was stable.

Conclusion

Perovskite-based $La_{1-x}Co_xMn_{1-y}Ni_yO_3$ ($x = 0.2$ and 0.4, $y = 0.1$, 0.3, and 0.5) have been developed as a H_2S gas sensor. When tested against H_2S, CO, NH_3, and LPG, as a function of operation temperature, $La_{0.6}CO_{0.4}MnO_3$ shows high sensor response towards H_2S gas at 280 °C. The material $La_{0.6}Co_{0.4}Mn_{0.5}Ni_{0.5}O_3$ shows high sensor response and high selectivity towards H_2S gas at 250 °C. 0.1 wt% Pd-doped $La_{0.6}Co_{0.4}Mn_{0.5}Ni_{0.5}O_3$ gave higher sensor response than the other compounds. This element has been tested for the H_2S gas concentration range 50–300 ppm at 200 °C. 0.1 wt% Pd-doped $La_{0.6}Co_{0.4}Mn_{0.5}Ni_{0.5}O_3$ can be expected as a promising material to be used as H_2S gas sensor at an operating temperature as low as 200 °C.

Fig. 11 Response characteristics of 0.1 wt% Pd-doped $La_{0.6}Co_{0.4}Mn_{0.5}Ni_{0.5}O_3$ calcined at 650 °C

References

1. Bie L-J, Yan X-N, Yin J, Duan Y-Q, Yuan Z-H (2007) Sens Actuator B: Chem 126:604
2. Wang Y, Mu Q, Wang G, Zhou Z (2010) Sens Actuator B: Chem 145:847
3. Khadayate RS, Waghulde RB, Wankhade MG, Sali JV, Patil PP (2007) Bull Mater Sci 30:129
4. Wang Y, Wang S, Zhao Y, Zhu B, Kong F, Wang D, Wu S, Huang W, Zhang S (2007) Sens Actuator B: Chem 125:79
5. Wagner T, Sauerwald T, Kohl C-D, Waitz T, Weidmann C, Tiemann M (2009) Thin Solid Films 517:6170
6. Shimizu K, Chinzei I, Nishiyama H, Kakimoto S, Sugaya S, Matsutani W, Satsuma A (2009) Sens Actuator B: Chem 141:410
7. Song P, Wang Q, Yang Z (2009) Sens Actuator B: Chem 141:109
8. Zhang L, Qin H, Song P, Hu J, Jiang M (2006) Mater Chem Phys 98:358
9. Skinner SJ (2001) Fuel Cells Bull 4:6
10. Kuroda K, Hashimoto I, Adachi K, Akikusa J, Tamou Y, Komada M, Ishihara T, Tskita Y (2000) Solid State Ionics 132:199
11. Brosha EL, Mukundan R, Brown DR, Garzon FH, Visser JH, Zanini M, Zhou Z, Logothetis EM (2000) Sens Actuators B 69:171
12. Delgado E, Michel CR (2006) Mater Lett 60:1613
13. Matsushima S, Maekawa T, Tamaki J, Miura N, Yamazoe N (1989) Role of additives on alcohol sensing by semiconductor gas sensor. Chem Lett 845–848
14. Xu C, Tamaki J, Miura N, Yamazoe N (1990) J Electrochem Soc Jpn 58:1143
15. Wagh MS, Jain GH, Patil DR, Patil SA, Patil LA (2006) Sens Actuator B 115:128
16. Wagh MS, Patil LA, Seth T, Amalnerkar DP (2004) Mater Chem Phys 84:228
17. Kanefusa S, Nitta M, Haradome M (1985) J Electrochem Soc 132:1770
18. Lantto V, Romppainen P (1988) J Electrochem Soc 135:2550
19. Yuanda W, Maosong T, Xiuli H, Yushu Z, Guorui D (2001) Sens Actuator B 79:187
20. Tamaki J, Yamada Y, Yamamoto Y, Matsuoka M, Ota I (2000) Sens Actuator B 66:70
21. Jain GH, Patil LA, Wagh MS, Patil DR, Patil SA, Amalnerkar DP (2006) Sens Actuato B 117:159
22. Xiangfeng C, Dongli J, Yu G, Chenmou Z (2006) Sens Actuator B 120:177
23. Gonga J, Chena Q, Lian M-R, Liu N-C, Stevenson RG, Adami F (2006) Sens Actuator B 114:32
24. Rezlescu E, Tudorache F, Popa P, Rezlescu N (2008) Sens Transducer J 91:100
25. Srivastava A, Jain K, Rashmi, Srivastava AK, Lakshmikumar ST (2006) Mater Chem Phys 97:85
26. Jayaraman V, Gnanasekar KI, Prabhu E, Gnanasekaran T, Periaswami G (1999) Sens Actuator B 55:175
27. Kiran J, Pant RP, Lakshmikumar ST (2006) Sens Actuator B 113:823
28. Ivanokskaya M, Bogdanov P (1998) Sens Actuator B 53:44
29. Bogdanov P, Ivanokskaya M, Comini E, Faglia G, Sherveglieri G (1999) Sens Actuator B 57:153
30. Yamazoe N (1991) Sens Actuator B 5:7
31. Mizsei J (1993) Sens Actuator B 15–16:328
32. Manorama SV, Gopal Reddy CV, Rao VJ, Lobo AS, Kulkarni SK (1999) Thin solid film 341:261
33. Nenov TG, Yordanov SP (1996) Ceramic sensors, technology and applications. Technomic Publication, Lancaster, pp. 137–138
34. Rothschild A, Komem Y (2004) Appl Phys 95:6374